Published in final edited form as:
Am J Physiol Cell Physiol. 2008 May ; 294(5): C1175–C1182. doi:10.1152/ajpcell.00049.2008.

Syncoilin is required for generating maximum isometric stress in skeletal muscle but dispensable for muscle cytoarchitecture

Jianlin Zhang[1,4,*], **Marie-Louise Bang**[1,5,*], **David S. Gokhin**[2], **Yingchun Lu**[1], **Li Cui**[3], **Xiaodong Li**[1], **Yusu Gu**[1], **Nancy D. Dalton**[1], **Maria Cecilia Scimia**[1,5], **Kirk L. Peterson**[1], **Richard L. Lieber**[2], and **Ju Chen**[1]

[1]Department of Medicine, University of California, San Diego, La Jolla

[2]Department of Orthopaedic Surgery and Bioengineering, University of California, San Diego and Veterans Affairs Medical Centers, San Diego

[3]Skaggs School of Pharmacy and Pharmaceutical Sciences, University of California, San Diego, La Jolla, California

[4]State Key Laboratory of Virology, Wuhan University, Wuhan, People's Republic of China

[5]Istituto di Ricovero e Cura a Carattere Scientifico, Scientific and Technology Pole, Multimedica, Milan, Italy

Abstract

Syncoilin is a striated muscle-specific intermediate filament-like protein, which is part of the dystrophin-associated protein complex (DPC) at the sarcolemma and provides a link between the extracellular matrix and the cytoskeleton through its interaction with α-dystrobrevin and desmin. Its upregulation in various neuromuscular diseases suggests that syncoilin may play a role in human myopathies. To study the functional role of syncoilin in cardiac and skeletal muscle in vivo, we generated syncoilin-deficient (*syncoilin*$^{-/-}$) mice. Our detailed analysis of these mice up to 2 yr of age revealed that syncoilin is entirely dispensable for cardiac and skeletal muscle development and maintenance of cellular structure but is required for efficient lateral force transmission during skeletal muscle contraction. Notably, *syncoilin*$^{-/-}$ skeletal muscle generates less maximal isometric stress than wild-type (WT) muscle but is as equally susceptible to eccentric contraction-induced injury as WT muscle. This suggests that syncoilin may play a supportive role for desmin in the efficient coupling of mechanical stress between the myofibril and fiber exterior. It is possible that the reduction in isometric stress production may predispose the syncoilin skeletal muscle to a dystrophic condition.

Keywords

intermediate filament; sarcomere; mutant mouse

The dystrophin-associated protein complex (DPC) in the striated muscle plasma membrane links the intracellular actin cytoskeleton with the extracellular matrix and provides mechanical stability to the membrane (14). In addition, the DPC is thought to play an important role in intracellular signaling, since mutations in members of the DPC have been associated with a variety of muscle disorders. The DPC is composed of three multiprotein complexes: the

Address for reprint requests and other correspondence: J. Chen, Dept. of Medicine, Univ. of California San Diego, 9500 Gilman Drive, BSB, Rm. 5025, La Jolla, CA 92093-0613 (juchen@ucsd.edu).
*J. Zhang and M.-L. Bang contributed equally to this work.

Present address of Y. Lu: 8438 Capricorn Way, Unit 12, San Diego, CA 92126.

dystroglycan complex, which binds to laminin in the extracellular matrix and dystrophin on the cytoplasmic side; the transmembrane sarcoglycan complex; and the cytoplasmic complex, composed of syntrophin and α-dystrobrevin (15,35). In addition to the interaction of α-dystrobrevin with the DPC components dystrophin, utrophin, and syntrophin (reviewed in Ref. 6), α-dystrobrevin has been shown to bind to dysbindin (5), synemin/desmuslin (24), DAMAGE (1), and syncoilin (26) [not to be confused with syncolin, a microtube-associated protein in erythrocytes (16) and syncollin, a secretory granule protein in pancreas and neutrophils (3,13)]. The specific functions of these proteins remain to be elucidated.

We focused on syncoilin, a 64-kDa intermediate filament-like protein specifically expressed in cardiac and skeletal muscle, where it is localized at the sarcolemma, the neuromuscular junction, the myotendinous junction, the sarcomeric Z line, and the perinuclear space (22,26). Unlike other intermediate filament proteins, syncoilin has a unique NH_2-terminal region with no known homology to any protein (26) and does not form homo- or heterodimers with other intermediate filaments (29). However, syncoilin binds to and colocalizes with the intermediate filament desmin and is thus thought to provide a link between the desmin intermediate filament network and the extracellular matrix through its binding to the DPC component α-dystrobrevin (29). Desmin is located around the Z line and is important for linking myofibrils together and connecting them to the sarcolemma and the nucleus. Deletion of desmin in mice results in loss of the lateral alignment of myofibrils, degeneration/regeneration cycles, and abnormal mitochondrial localization, demonstrating its important role in maintaining the structural integrity of muscle (19,23,32). This was manifested by a reduction in isometric stress production but surprisingly less susceptibility to damage when muscles were subjected to eccentric contractions (31). In desmin-deficient mice, syncoilin protein was reduced and completely lost from neuromuscular junctions and around Z lines and was redistributed from the sarcolemma to the cytoplasm, suggesting that syncoilin's cytoskeletal location and, partly, its sarcolemmal localization depend on desmin (22). Syncoilin transcript levels were unchanged, implying that the reduction in syncoilin protein in the absence of desmin is due to posttranscriptional regulation by either decreased protein translation or protein degradation. The upregulation of syncoilin in dystrophic muscle in various forms of human neuromuscular disease (8,18), as well as in both α-dystrobrevin knockout (22) and dystrophin-deficient *mdx* mice (26,34), further raises the possibility that syncoilin may play a role in human skeletal muscle and cardiac diseases. However, its function remains elusive.

To study the functional role of syncoilin in cardiac and skeletal muscle in vivo, we generated syncoilin-deficient (*syncoilin*$^{-/-}$) mice. Although our detailed analysis of these mice revealed that syncoilin is dispensable for basal striated muscle function, assembly of muscle cytoarchitecture, and synthesis and localization of DPC constituents, *syncoilin*$^{-/-}$ skeletal muscle generated lower isometric stress during contraction, a characteristic of almost all myopathic muscles (11,21,27,31).

Materials and Methods

Generation of syncoilin knockout mice

Genomic DNA clones were isolated from a mouse 129-SVJ genomic DNA library (Stratagene, La Jolla, CA) by screening using a full-length syncoilin probe. A point mutation was introduced into the 3′ splice site of exon 2 together with the neomycin resistance gene (Fig. 1A), which was expected to result in ablation of syncoilin mRNA due to aberrant RNA splicing. The targeting construct was verified by sequencing and linearized with *Not*I before electroporation into 129-SVJ-derived embryonic stem (ES) cells at the Transgenic Core Facility at the University of California, San Diego. G418-resistant ES clones were screened for homologous recombination by Southern blot analysis with the probe shown in Fig. 1B. The wild-type (WT) allele is represented by the band of 9.5 kb, whereas the 7.5-kb band represents the correctly

targeted mutant allele. Cells from two independent targeted clones were microinjected into C57BL/B6 blastocysts and transferred into pseudopregnant mice. Male chimeras resulting from the microinjections were inbred with female Black Swiss mice to generate germ line-transmitted heterozygous mice. These were subsequently intercrossed to generate homozygous mice. Offspring from intercrosses were genotyped by PCR analysis using mouse tail DNA and WT and mutant allele-specific primers. The following primers were used: syncoilin WT (sense: GGCAGCTCCAACTTCAGAAC; reverse: AGCCAGGGCTACACAGAGAG) and mutant (sense: AATGGGCTGACCGCTTCCTCGT; reverse: TCCAGGCCAACCTGAACTAC). All animal studies were performed using Laboratory Animal Care and Use Committee-approved protocols and conformed to the *Guide for the Care and Use of Laboratory Animals*, published by the National Institutes of Health (NIH Publication No. 85-23, Revised 1996).

RNA analyses

Total RNA was isolated from mouse skeletal muscle and heart tissue using Trizol reagent (Invitrogen) according to the manufacturer's instructions. For RT-PCR analysis, first-strand cDNA synthesis was performed with the random primer and SuperScript kit (Invitrogen). The cDNA was utilized as a PCR template to perform PCR using specific primers for *syncoilin* exon 2-3 (forward: AGAGCCGCCAGGGCCTGGAGGAGG; reverse: TGTGGAAAGCTCTTCAGCAAGGCTCATC). For dot-blot analysis, 2 μg of RNA were spotted in triplicate onto nylon membranes using a Hybri-dot manifold (Bethesda Research Laboratories, Gaithersburg, MD). Membranes were subsequently probed with [γ-^{32}P]dATP end-labeled cDNA probes for GAPDH, atrial natriuretic factor (ANF), α-myosin heavy chain (α-MHC), β-MHC, cardiac actin, and skeletal actin by using QuickHyb solution (Stratagene) following the manufacturer's instructions.

Protein isolation and Western blot analysis

Total protein extracts were prepared from heart and skeletal muscle, separated on 4–12% gels (Bio-Rad), and subjected to Western blot analysis using antibodies against full-length syncoilin [1:250, SYNC-FP (26)], NH_2-terminal syncoilin (1: 250), α1-dystrobrevin [1:100, α1CT-FP (7)] (kindly provided by Kay E. Davies), desmin (1:1,000, Ab-8592; Abcam), sarcomeric α-actinin EA-53 (1:1,000; Sigma-Aldrich, St. Louis, MO), dystrophin (1:100, NCL-DYS1; Novus Biologicals), utrophin (1:200, sc-15377; Santa Cruz Biotechnology), β-dystroglycan [1:40, MANDAG2 clone 7D11; Developmental Studies Hybridoma Bank (DSHB), University of Iowa, Iowa City, IA], and sarcoglycan (1:20, NCL-a-SARC; Novocastra). GAPDH antibodies were used for normalization (1: 1,000; Sigma-Aldrich).

Histology

Mouse heart and skeletal muscle were dissected out and fixed with 4% paraformaldehyde, followed by dehydration and paraffin embedding. Sections (10 μm) were analyzed by staining with hematoxylin and eosin or by Masson's trichrome method.

Immunostaining

Immunostainings of isolated adult cardiomyocytes and frozen sections of tibialis anterior (TA) muscle were performed. Cardiomyocytes were isolated essentially as described previously (12). Briefly, hearts were cannulated and mounted on a Langendorff perfusion apparatus and perfused with Ca^{2+}-free Tyrode solution (in mM: 121 NaCl, 5 $NaHCO_3$, 10 HEPES, 4.7 KCl, 1.2 KH_2PO_4, 1 $MgCl_2$, 1.2 $MgSO_4$, 15 glucose, and 30 taurine, pH 7.4) for 10 min at 37°C. Perfusion was then switched to the same solution containing 1 mg/ml collagenase type II (Worthington) for about 10 min until the heart became flaccid. Subsequently, the heart was removed and cells were dissociated. Ca^{2+}-free Tyrode solution containing 4% bovine serum albumin (fraction V; Sigma) was then added to the cell suspension, and the cells were allowed

to settle. After resuspension in Ca^{2+}-free Tyrode solution, cells were plated on laminin (20 mg/ml; Upstate Biotechnology) precoated cover slides. After settling for about 1 h, cells were fixed for 5 min with 4% paraformaldehyde in PBS and subsequently rinsed with PBS. For frozen TA muscle sections, hindlimbs were transected midfemur and pinned to cork with the knee joint fixed at 90° and the ankle joint fixed at 180° (fully plantarflexed), resulting in stretching of the TA muscle. After being fixed overnight, the TA muscle was dissected out and incubated in 10, 15, and 30% sucrose in PBS before being frozen in OCT. Longitudinal frozen sections (10 μm) of TA muscle or isolated cardiomyocytes were permeabilized and blocked in a solution containing 1% normal goat serum, 0.3% Triton X-100, 50 mM glycine, and 1% cold water fish gelatin (Sigma-Aldrich) in 1× PBS for 30 min, followed by incubation overnight at 4°C in a humidified chamber with the primary antibody in wash buffer (0.01% Triton X-100, 5 mM glycine, 0.1% fish gelatin in PBS). The following primary antibodies were used: α1-dystrobrevin (1:75; kindly provided by Kay E. Davies), desmin (1:75, Ab-8592; Abcam), sarcomeric α-actinin EA-53 (1:1,000; Sigma-Aldrich), α-myosin F59 (1:50; DSHB), dystrophin (1:500, Sc-15376; Santa Cruz Biotechnology), and β-dystroglycan (1:100, MANDAG2 clone 7D11; DSHB). After being rinsed in wash buffer, sections were incubated at room temperature for 4 h with phalloidin (1:100; Sigma-Aldrich) and/or fluorescently labeled secondary antibodies (goat anti-mouse FITC, goat anti-rabbit FITC, or goat anti-mouse RedX antibody; Sigma-Aldrich) at a final dilution of 1:100 in wash buffer. Slides were rinsed in wash buffer, dried, and mounted in Gelvatol. Confocal microscopy was performed using a Bio-Rad Radiance 2000 system with a ×60 Plan-apochromat 1.4 N.A. objective (Zeiss). Individual images (1,024 × 1,024) were converted to TIFF format and merged as pseudocolor RGB images using Imaris (Bit-plane).

Transmission electron microscopy

For transmission electron microscopy (TEM), mice were injected with heparin (0.5 ml, 100 U/ml) and subsequently anesthetized with Nembutal (40 μl, 50 mg/μl) and placed in a position where the knee joint was fixed at 90° and the ankle joint at 180° (fully plantarflexed), resulting in stretching of the TA muscle. The chest was then opened to expose the heart, and the right atrium was cut off. The mice were perfused though the left ventricle with 30 mM KCl in Tyrode solution (100 mM NaCl, 30 mM KCl, 1 mM $MgCl_2 \cdot 6H_2O$, 4 mM $NaHCO_3$, 10 mM HEPES, and 5.5 mM glucose, pH 7.4), followed by fixative (2% paraformaldehyde, 2% glutaraldehyde in 0.15 M sodium cacodylate buffer, pH 7.4). Subsequently, heart and TA muscles were dissected out and kept in fixative overnight. Tissue was then cut into small pieces (~1-mm cubes) and stained overnight in 1% osmium tetroxide, 0.8% potassium ferrocyanide. The following day, tissue was stained for 2 h in 2% uranyl acetate and subsequently dehydrated in a series of ethanol and acetone washes. The tissue was embedded in Durcupan resin (EMD, Gibbstown, NJ), and ultrathin sections (60–70 nm) were stained with lead citrate. Electron micrographs were recorded using a JEOL 1200EX electron microscope operated at 80 kV.

Echocardiography

Mice were anesthetized with isoflurane, and transthoracic echocardiography was performed before and 14 days after transverse aortic constriction (TAC) as described in detail elsewhere (33).

Hemodynamic measurements

Cardiac function of the left ventricle was measured by high-fidelity microsonometry in mice as described previously (2). The effects of the β-adrenergic agonist dobutamine (0.75, 2, and 4 $\mu g \cdot kg^{-1} \cdot min^{-1}$) were also determined.

Microsurgical techniques to introduce pressure overload cardiac hypertrophy

Left ventricular pressure overload was produced in mice by performing TAC as described previously (30). At 14 days following surgery, the pressure gradient generated by aortic banding was measured by introducing high-fidelity pressure transducers into the left and right common carotids. Only mice showing an adequate pressure gradient (>40 mmHg) were included in the analysis.

Exercise capacity test

Mice were subjected to an exercise treadmill test until exhaustion. Each mouse was tested on a 25% inclined custom-made single-lane treadmill, supplied with stainless steel grids at the end of the lane with electrical stimulus of 0.25 mA, 1 Hz, and 200 ms. After having been exposed to the equipment and treadmill running twice before, the mice were warmed up for 10 min at 0.15 m/s. The speed was subsequently increased by 0.05 m/s every 2 min. The time to exhaustion was recorded when the mouse remained on the steel grids and could not continue running despite gentle prodding.

Active mechanics and eccentric contraction-induced injury

Mice were killed by cervical dislocation, and the fifth toe muscle of the multibellied extensor digitorum longus (EDL) from each mouse hindlimb was microdissected in Ringer solution (137 mM NaCl, 5 mM KCl, 24 mM NaH_2PO_4, 2 mM $CaCl_2$, 1 mM $MgSO_4$, 11 mM glucose, and 1 mg/l curare). The fifth toe was chosen because of its fiber length homogeneity, mixed fiber-type distribution, and distinct origin and insertion tendons (9). EDL muscles were transferred to a customized muscle-testing chamber and subjected to the testing protocol previously described in detail (31). Briefly, after muscles were secured in a testing apparatus, muscle length was adjusted by laser diffraction to a sarcomere length of ~3.0 μm. Passive mechanical properties were measured by imposing a 10% fiber length (L_f) stretch at a rate of 0.7 L_f/s, repeated three times at 3-min intervals. Maximum isometric tension was then measured by applying a 400-ms train of 0.3-ms pulses delivered at 100 Hz while muscle length was held constant. This measurement was repeated twice at 5 min intervals. Next, each muscle underwent a series of 10 eccentric contractions, one every 3 min to minimize fatigue effects. Isometric contractions and passive stretches were then repeated. This protocol was performed on only one hindlimb per mouse, because the contralateral muscle had deteriorated by the time experimentation on one hindlimb was complete. Muscle mass, density, and starting L_f were used to compute the physiological cross-sectional area of each EDL muscle to normalize the isometric tension values as previously described (20).

Passive mechanics of single muscle fibers

Evaluation of passive mechanical properties was performed on single muscle fibers of the EDL by using an approach adapted from methods described previously (4,17). Briefly, after death, the EDL was promptly dissected from each hindlimb and maintained in storage solution at −20°C for up to 3 wk. At the time of mechanical testing, EDL muscles were removed from the storage solution and placed in relaxing solution [59.4 mM imidazole, 86 mM KCH_4O_3S, 0.13 mM $Ca(KCH_4O_3S)_2$, 10.8 mM $Mg(KCH_4O_3S)_2$, 5.5 mM K_3EDTA, 1 mM KH_2PO_4, 5.1 mM Na_2ATP, and 50 mm leupeptin]. Single fiber segments were carefully dissected, transferred to a mechanical testing chamber filled with relaxing solution, and secured to a force transducer and a motor. Sarcomere length was measured by transilluminating the fiber with a laser and projecting the diffraction pattern onto a photodiode array above the fiber. Muscle fibers were stretched to failure in 250-μm increments with the use of a micrometer attached to the motor, with a 2-min rest between increments to minimize confounding stress relaxation effects. Sarcomere length and passive tension were recorded at the end of each 2-min interval, and the

slope of the resulting stress-strain curve (Young's modulus) was computed using linear regression. This protocol was performed in triplicate for fibers within each EDL muscle.

Statistical analysis

Data are averages ± SD or SE. Statistical comparisons between WT and *syncoilin*$^{-/-}$ mice were done using unpaired Student's *t*-test. A P value <0.05 is considered significant.

Results

Generation of syncoilin knockout mice

To study the functional role of syncoilin in vivo, we generated *syncoilin*$^{-/-}$ mice by gene targeting. A point mutation was introduced in the 3′ splice site of exon 2 together with the neomycin resistance gene (Fig. 1A), which was expected to result in ablation of syncoilin mRNA due to aberrant RNA splicing. The linearized targeting vector was electroporated into 129-SVJ-derived ES cells, and homologous recombinant clones were identified by Southern blot analysis (Fig. 1B) using the primer indicated in Fig. 1A. Two identified independent homologous recombinant ES cells were injected into blastocysts from C57/B6 mice and gave rise to chimeric mice that were then bred with Black Swiss mice to generate germ line-transmitted heterozygous *syncoilin*$^{+/-}$ mice. These mice were subsequently mated to generate homozygous *syncoilin*$^{-/-}$ mice as determined by PCR. Successful ablation of the *syncoilin* gene was confirmed by RT-PCR on RNA from heart, muscle, and liver using primers located in exons 2 and 3 (Fig. 1B). In addition, Western blot analyses using polyclonal antibodies against both full-length syncoilin and NH_2-terminal syncoilin (Fig. 1D) detected no residual syncoilin protein in *syncoilin*$^{-/-}$ mice.

Syncoilin$^{-/-}$ mice have normal cardiac and skeletal muscle morphology

Syncoilin$^{-/-}$ mice were born in Mendelian ratios, were fertile, and survived until adulthood without any obvious abnormalities. The heart weight-to-body weight ratio was normal, and histological analysis by hematoxylin and eosin staining of cardiac and skeletal muscle paraffin sections showed no cardiac or skeletal muscle abnormalities in *syncoilin*$^{-/-}$ mice up till 1 yr of age (Supplemental Fig. 1 and data not shown). (Supplemental data for this article is available online at the *American Journal of Physiology-Cell Physiology* website.) Trichrome staining also detected no fibrosis in either skeletal or heart muscle from *syncoilin*$^{-/-}$ mice (data not shown). In skeletal muscle, no signs of centralized nuclei, necrosis, increased fiber size variability, abnormal fiber shape, or altered fiber density were found in *syncoilin*$^{-/-}$ compared with WT mice (data not shown). In addition, myosin ATPase staining revealed no significant differences in the size of either type 1 or type 2 fibers between genotypes, and there were no statistically significant differences in the fiber type distribution between the two groups as determined by SDS-PAGE measurements of different isoforms of the myosin heavy chain (Fig. 2).

No abnormalities in protein expression or localization in *syncoilin*$^{-/-}$ mice

To determine whether ablation of syncoilin resulted in changes in the expression levels of other cytoskeletal proteins associated with syncoilin, the DPC, or the sarcomere, we performed Western blot analyses on cardiac and skeletal muscle lysates from 8-wk-old *syncoilin*$^{-/-}$ mice and WT littermates. As shown in Fig. 3A, no changes in protein expression levels of α1-dystrobrevin, desmin, dystrophin, utrophin, β-dystroglycan, and sarcoglycan were found in *syncoilin*$^{-/-}$ compared with WT heart and skeletal muscle. We also performed immunostainings to determine whether the localizations of these proteins were affected by the absence of syncoilin. This revealed no differences in the localization of α-actinin, actin, myosin,

α1-dystrobrevin, desmin, dystrophin, and β-dystroglycan in TA muscle (Fig. 3B) and isolated cardiomyocytes (data not shown).

No ultrastructural abnormalities in *syncoilin*$^{-/-}$ striated muscle sarcomeres and cardiac intercalated disks

To determine whether ablation of *syncoilin* resulted in any ultrastructural abnormalities, we performed TEM on left ventricle and TA muscle from 3-mo-old *syncoilin*$^{-/-}$ mice and WT control littermates. As shown in Fig. 4, *syncoilin*$^{-/-}$ skeletal and cardiac muscle had normal ultrastructural organization with well-aligned and organized sarcomeres. Also, no abnormalities were found in the cardiac intercalated disk, a structure important for mechanical coupling of cardiomyocytes (28).

Syncoilin$^{-/-}$ mice have normal cardiac function

To determine the effect of syncoilin deficiency on cardiac function, we performed noninvasive echocardiography on 8-wk-old *syncoilin*$^{-/-}$ mice. As shown in Table 1, no significant differences between *syncoilin*$^{-/-}$ mice and WT control mice were found in regard to left ventricular chamber dimensions, fractional shortening, and heart rate. Likewise, hemodynamic function as assessed by cardiac catheterization in the absence or presence of graded doses of dobutamine of 10-wk-old and 20-mo-old mice revealed no significant differences in contractile function between *syncoilin*$^{-/-}$ and WT mice both at baseline and in the presence of dobutamine (Table 2 and data not shown). To determine the response of *syncoilin*$^{-/-}$ mice to cardiac stress, we performed TAC on 8-wk-old mice to induce pressure overload-induced hypertrophy. Cardiac function before and after 14 days of TAC was evaluated using echocardiography, and pressure gradients generated by the aortic constriction were measured. As shown in Table 1, similar pressure gradients were produced in both groups. After TAC, left ventricular wall thickness and mass and mRNA levels of hypertrophy-induced genes were increased by similar amounts in both groups (Table 1 and data not shown), indicating that the response to hypertrophic stimuli is unaffected in *syncoilin*$^{-/-}$ mice.

Syncoilin$^{-/-}$ skeletal muscle generates lower isometric stress compared with WT but shows a normal response to eccentric contraction-induced injury

Isometric stress production and passive tension before and after injury induced by cyclic eccentric contractions in the fifth toe muscle of the multibellied mouse EDL muscle were measured in 10-wk-old *syncoilin*$^{-/-}$ and WT mice (31). Results showed significantly lower isometric stress production in *syncoilin*$^{-/-}$ mice compared with WT mice; however, despite the lower stress production, *syncoilin*$^{-/-}$ skeletal muscle still exhibited the same vulnerability to eccentric contraction-induced injury as WT, when “injury” was defined as a reduction in maximum isometric stress across the eccentric exercise bout (Fig. 5, A and B).

Syncoilin$^{-/-}$ muscle has normal passive mechanical properties and exercise capacity

Passive tensile stress in whole fifth toe muscles from the EDL subjected to 10% stretch measured before and after the eccentric injury protocol showed no significant differences, although the whole muscle passive stress in *syncoilin*$^{-/-}$ muscle was ~25% lower than in WT (Fig. 5C). This difference was not quite significant before the EC protocol ($P = 0.1$) or after the protocol ($P > 0.3$). Passive tensile testing (4,17) on single fibers isolated from the EDL muscle from 10-wk-old *syncoilin*$^{-/-}$ mice and WT controls also showed no differences in the elastic modulus (Young's modulus) as measured from the slope of the stress-strain curve as fibers were incrementally stretched in 250-μm steps (Fig. 5D). Finally, we tested the exercise capacity of *syncoilin*$^{-/-}$ compared with WT mice in treadmill tests to exhaustion but found no significant differences in performance between the two groups (Fig. 5E).

Discussion

Syncoilin is a striated muscle-specific intermediate filament-like protein that is part of the DPC and links the complex to the cytoskeleton through its interaction with α-dystrobrevin and desmin (26,29). Furthermore, its upregulation in various neuromuscular diseases (8,18) has suggested that syncoilin may be involved in muscular myopathies. We studied the in vivo role of syncoilin by the generation and detailed analysis of cardiac and skeletal muscle from *syncoilin*$^{-/-}$ mice up to 2 yr of age using histological, TEM, biochemical, molecular, biophysical, and physiological tools. Our data suggest that syncoilin is dispensable for the development and maintenance of cardiac and skeletal muscle structure and integrity. Syncoilin deficiency also did not affect cardiac and skeletal muscle function, either at basal conditions or following various forms of stress, such as pressure-induced cardiac hypertrophy, exercise to exhaustion, and eccentric contraction-induced injury in skeletal muscle. However, *syncoilin*$^{-/-}$ mice had a significant reduction in maximum isometric stress generation in skeletal muscle, suggesting its role in efficient lateral force transmission during skeletal muscle contraction. Although no histological or ultrastructural abnormalities were found in *syncoilin*$^{-/-}$ mice at any developmental stage studied, it is possible that the reduction in isometric stress production may predispose *syncoilin*$^{-/-}$ skeletal muscle to a dystrophic condition. It is important to point out that low stress production is characteristic for almost all myopathic muscles whether the underlying basis for the dystrophy is mutations in dystrophin (11,21,25), desmin (31), or members of the DPC (27). However, in contrast to these mouse models, *syncoilin*$^{-/-}$ skeletal muscle responds normally to eccentric contraction-induced injury.

Recent studies have suggested that syncoilin may play an important role in organizing and linking the desmin-associated intermediate filament system to the extracellular matrix via the DPC (29). However, no abnormalities in the organization or location of DPC components or the desmin intermediate filament system were observed in *syncoilin*$^{-/-}$ mice, indicating that syncoilin is not required for the structural organization of striated muscle or the correct localization of desmin. Thus desmin must be targeted to the sarcolemma and neuromuscular junction through its interaction with additional unidentified sarcolemmal components. However, it is possible that syncoilin may reinforce and stabilize desmin's connection to the sarcolemma. Ablation of desmin in mice previously has been shown to result in decreased maximal isometric stress production, suggesting that interconnections between sarcomeres along and across muscle fibers are important for efficient transfer of mechanical stress from the myofibril to the fiber exterior (31). The downregulation and redistribution of syncoilin from the cytoskeleton to the cytoplasm in *desmin*$^{-/-}$ mice (22) together with the reduction in isometric stress production in *syncoilin*$^{-/-}$ muscle suggests that syncoilin may play a supportive role for desmin in mediating efficient stress production. *Desmin*$^{-/-}$ mice have been shown to be more resistant to mechanical injury compared with WT mice (31), which was attributed to more compliant intermyofibrillar connections in *desmin*$^{-/-}$ muscle, permitting a greater degree of sliding of adjacent myofibrils relative to one another in response to eccentric contractions, thus resulting in less stress on adjacent myofibrils and consequently less injury. On the other hand, *mdx* mice and *mdx/utrophin*$^{-/-}$ mice have been reported to be highly susceptible to eccentric contraction-induced injury, most likely due to increased membrane fragility and associated damage (10,25). In *syncoilin*$^{-/-}$ mice, the drop in maximum isometric tension after cyclic eccentric contractions was similar to that observed in WT mice. Thus the absence of syncoilin does not seem to affect membrane stability, which is in agreement with our results showing that syncoilin deficiency does not result in any histological abnormalities or affect the localization or expression of other members of the DPC. Conversely, the failure of syncoilin deficiency to protect against mechanical injury as observed in *desmin*$^{-/-}$ mice suggests that syncoilin does not play the typical role of other intermediate filaments in forming intermyofibrillar connections, which is consistent with the inability of syncoilin to form homo-

and heterodimers with other intermediate filaments. Instead, syncoilin may play a supportive role for desmin in efficiently coupling the myofibril and the fiber exterior.

In summary, our data demonstrate that syncoilin is dispensable for cardiac and skeletal muscle development and maintenance of cellular structure but is required for efficient lateral force transmission during skeletal muscle contraction.

Supplementary Material

Refer to Web version on PubMed Central for supplementary material.

Acknowledgments

Grants: This work was supported by National Institutes of Health (NIH) Grants (to J. Chen and R. L. Lieber). TEM was carried out at the National Center for Microscopy and Imaging Research, which is supported by NIH Grant RR04050 (to M. H. Ellisman).

References

1. Albrecht DE, Froehner SC. DAMAGE, a novel α-dystrobrevin-associated MAGE protein in dystrophin complexes. J Biol Chem 2004;279:7014–7023. [PubMed: 14623885]
2. Arber S, Hunter JJ, Ross J Jr, Hongo M, Sansig G, Borg J, Perriard JC, Chien KR, Caroni P. MLP-deficient mice exhibit a disruption of cardiac cytoarchitectural organization, dilated cardiomyopathy, and heart failure. Cell 1997;88:393–403. [PubMed: 9039266]
3. Bach JP, Borta H, Ackermann W, Faust F, Borchers O, Schrader M. The secretory granule protein syncollin localizes to HL-60 cells and neutrophils. J Histochem Cytochem 2006;54:877–888. [PubMed: 16517980]
4. Barash IA, Bang ML, Mathew L, Greaser ML, Chen J, Lieber RL. Structural and regulatory roles of muscle ankyrin repeat protein family in skeletal muscle. Am J Physiol Cell Physiol 2007;293:C218–C227. [PubMed: 17392382]
5. Benson MA, Newey SE, Martin-Rendon E, Hawkes R, Blake DJ. Dysbindin, a novel coiled-coil-containing protein that interacts with the dystrobrevins in muscle and brain. J Biol Chem 2001;276:24232–24241. [PubMed: 11316798]
6. Blake DJ. Dystrobrevin dynamics in muscle-cell signalling: a possible target for therapeutic intervention in Duchenne muscular dystrophy? Neuromuscul Disord 2002;12:S110–S117. [PubMed: 12206805]
7. Blake DJ, Nawrotzki R, Loh NY, Gorecki DC, Davies KE. β-Dystrobrevin, a member of the dystrophin-related protein family. Proc Natl Acad Sci USA 1998;95:241–246. [PubMed: 9419360]
8. Brown SC, Torelli S, Ugo I, De Biasia F, Howman EV, Poon E, Britton J, Davies KE, Muntoni F. Syncoilin upregulation in muscle of patients with neuromuscular disease. Muscle Nerve 2005;32:715–725. [PubMed: 16124004]
9. Chleboun GS, Patel TJ, Lieber RL. Skeletal muscle architecture and fiber-type distribution with the multiple bellies of the mouse extensor digitorum longus muscle. Acta Anat (Basel) 1997;159:147–155. [PubMed: 9575365]
10. Deconinck N, Rafael JA, Beckers-Bleukx G, Kahn D, Deconinck AE, Davies KE, Gillis JM. Consequences of the combined deficiency in dystrophin and utrophin on the mechanical properties and myosin composition of some limb and respiratory muscles of the mouse. Neuromuscul Disord 1998;8:362–370. [PubMed: 9713852]
11. Dellorusso C, Crawford RW, Chamberlain JS, Brooks SV. Tibialis anterior muscles in mdx mice are highly susceptible to contraction-induced injury. J Muscle Res Cell Motil 2001;22:467–475. [PubMed: 11964072]
12. DeSantiago J, Maier LS, Bers DM. Frequency-dependent acceleration of relaxation in the heart depends on CaMKII, but not phospholamban. J Mol Cell Cardiol 2002;34:975–984. [PubMed: 12234767]

13. Edwardson JM, An S, Jahn R. The secretory granule protein syncollin binds to syntaxin in a Ca^{2+}-sensitive manner. Cell 1997;90:325–333. [PubMed: 9244306]
14. Ervasti JM, Campbell KP. A role for the dystrophin-glycoprotein complex as a transmembrane linker between laminin and actin. J Cell Biol 1993;122:809–823. [PubMed: 8349731]
15. Ervasti JM, Campbell KP. Membrane organization of the dystrophin-glycoprotein complex. Cell 1991;66:1121–1131. [PubMed: 1913804]
16. Feick P, Foisner R, Wiche G. Immunolocalization and molecular properties of a high molecular weight microtubule-bundling protein (syncolin) from chicken erythrocytes. J Cell Biol 1991;112:689–699. [PubMed: 1993737]
17. Friden J, Lieber RL. Spastic muscle cells are shorter and stiffer than normal cells. Muscle Nerve 2003;27:157–164. [PubMed: 12548522]
18. Howman EV, Sullivan N, Poon EP, Britton JE, Hilton-Jones D, Davies KE. Syncoilin accumulation in two patients with desmin-related myopathy. Neuromuscul Disord 2003;13:42–48. [PubMed: 12467731]
19. Li Z, Mericskay M, Agbulut O, Butler-Browne G, Carlsson L, Thornell LE, Babinet C, Paulin D. Desmin is essential for the tensile strength and integrity of myofibrils but not for myogenic commitment, differentiation, and fusion of skeletal muscle. J Cell Biol 1997;139:129–144. [PubMed: 9314534]
20. Lieber RL, Friden J. Functional and clinical significance of skeletal muscle architecture. Muscle Nerve 2000;23:1647–1666. [PubMed: 11054744]
21. Lynch GS, Hinkle RT, Chamberlain JS, Brooks SV, Faulkner JA. Force and power output of fast and slow skeletal muscles from mdx mice 6–28 months old. J Physiol 2001;535:591–600. [PubMed: 11533147]
22. McCullagh KJ, Edwards B, Poon E, Lovering RM, Paulin D, Davies KE. Intermediate filament-like protein syncoilin in normal and myopathic striated muscle. Neuromuscul Disord. 2007
23. Milner DJ, Weitzer G, Tran D, Bradley A, Capetanaki Y. Disruption of muscle architecture and myocardial degeneration in mice lacking desmin. J Cell Biol 1996;134:1255–1270. [PubMed: 8794866]
24. Mizuno Y, Thompson TG, Guyon JR, Lidov HG, Brosius M, Imamura M, Ozawa E, Watkins SC, Kunkel LM. Desmuslin, an intermediate filament protein that interacts with α-dystrobrevin and desmin. Proc Natl Acad Sci USA 2001;98:6156–6161. [PubMed: 11353857]
25. Moens P, Baatsen PH, Marechal G. Increased susceptibility of EDL muscles from mdx mice to damage induced by contractions with stretch. J Muscle Res Cell Motil 1993;14:446–451. [PubMed: 7693747]
26. Newey SE, Howman EV, Ponting CP, Benson MA, Nawrotzki R, Loh NY, Davies KE, Blake DJ. Syncoilin, a novel member of the intermediate filament superfamily that interacts with α-dystrobrevin in skeletal muscle. J Biol Chem 2001;276:6645–6655. [PubMed: 11053421]
27. Patel ND, Jannapureddy SR, Hwang W, Chaudhry I, Boriek AM. Altered muscle force and stiffness of skeletal muscles in alpha-sarcoglycan-deficient mice. Am J Physiol Cell Physiol 2003;284:C962–C968. [PubMed: 12620894]
28. Perriard JC, Hirschy A, Ehler E. Dilated cardiomyopathy: a disease of the intercalated disc? Trends Cardiovasc Med 2003;13:30–38. [PubMed: 12554098]
29. Poon E, Howman EV, Newey SE, Davies KE. Association of syncoilin and desmin: linking intermediate filament proteins to the dystrophin-associated protein complex. J Biol Chem 2002;277:3433–3439. [PubMed: 11694502]
30. Rockman HA, Ono S, Ross RS, Jones LR, Karimi M, Bhargava V, Ross J Jr, Chien KR. Molecular and physiological alterations in murine ventricular dysfunction. Proc Natl Acad Sci USA 1994;91:2694–2698. [PubMed: 8146176]
31. Sam M, Shah S, Friden J, Milner DJ, Capetanaki Y, Lieber RL. Desmin knockout muscles generate lower stress and are less vulnerable to injury compared with wild-type muscles. Am J Physiol Cell Physiol 2000;279:C1116–C1122. [PubMed: 11003592]
32. Shah SB, Su FC, Jordan K, Milner DJ, Friden J, Capetanaki Y, Lieber RL. Evidence for increased myofibrillar mobility in desmin-null mouse skeletal muscle. J Exp Biol 2002;205:321–325. [PubMed: 11854369]

33. Tanaka N, Dalton N, Mao L, Rockman HA, Peterson KL, Gottshall KR, Hunter JJ, Chien KR, Ross J Jr. Transthoracic echocardiography in models of cardiac disease in the mouse. Circulation 1996;94:1109–1117. [PubMed: 8790053]

34. Wilding JR, Schneider JE, Sang AE, Davies KE, Neubauer S, Clarke K. Dystrophin- and MLP-deficient mouse hearts: marked differences in morphology and function, but similar accumulation of cytoskeletal proteins. FASEB J 2005;19:79–81. [PubMed: 15494447]

35. Yoshida M, Suzuki A, Yamamoto H, Noguchi S, Mizuno Y, Ozawa E. Dissociation of the complex of dystrophin and its associated proteins into several unique groups by *n*-octyl β-d-glucoside. Eur J Biochem 1994;222:1055–1061. [PubMed: 8026484]

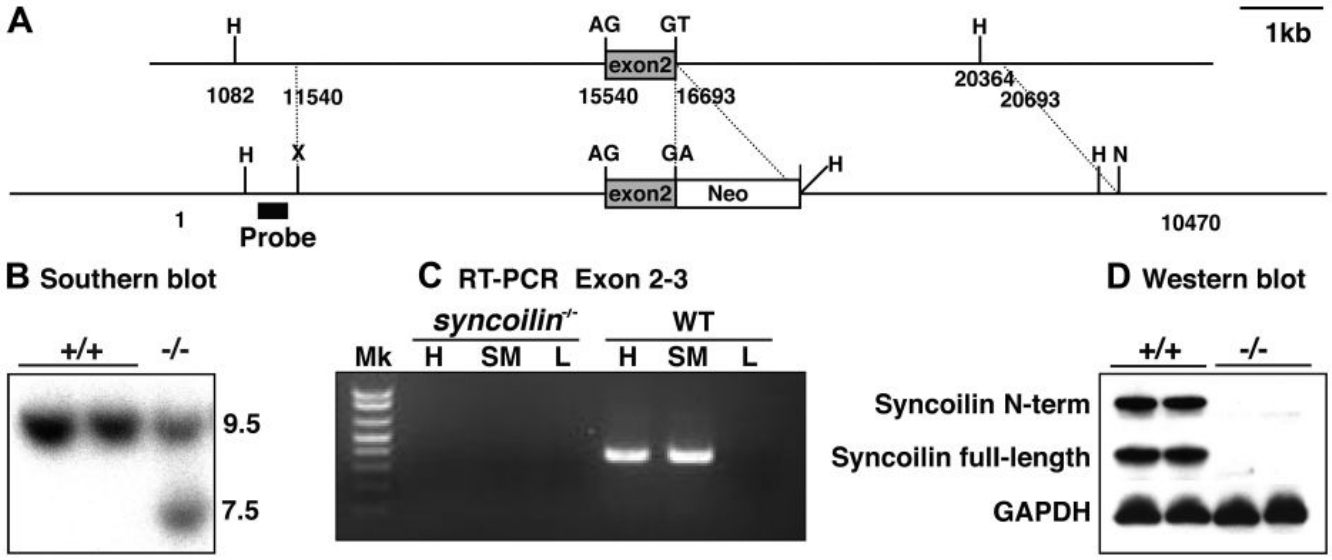

Fig. 1.

Targeting of the *syncoilin* gene. *A*: targeting strategy for generation of syncoilin knockout mice. A restriction map of the relevant genomic region of *syncoilin* is shown at *top*, and the mutated locus after recombination is shown at *bottom*. Dashed lines indicate the genomic segment included in the targeting construct. H, *Hin*dIII; X, *Xho*I; N, *Not*I. *B*: detection of wild-type (+/+) and targeted alleles (−/−) by Southern blot analysis after digestion with *Hin*dIII. *C*: RT-PCR analysis confirming the successful knockout of syncoilin. H, heart; SM, skeletal muscle; L, liver; Mk, molecular weight marker; WT, wild type. *D*: Western blot analysis using antibodies against N-terminal and full-length syncoilin.

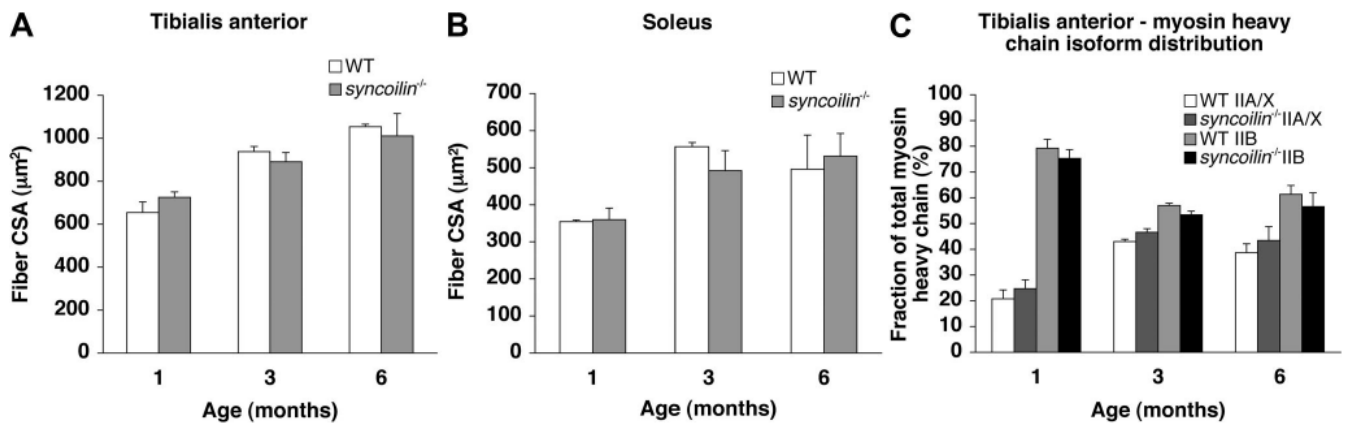

Fig. 2.

Fiber sizes and myosin heavy chain distribution. Fiber cross-sectional area (CSA) in tibialis anterior (TA; *A*) and soleus muscle (*B*) from 1-, 3-, and 6-mo-old WT and *syncoilin*$^{-/-}$ mice. *C*: myosin heavy chain isoform distribution in 1-, 3-, and 6-mo-old WT and *syncoilin*$^{-/-}$ TA muscle.

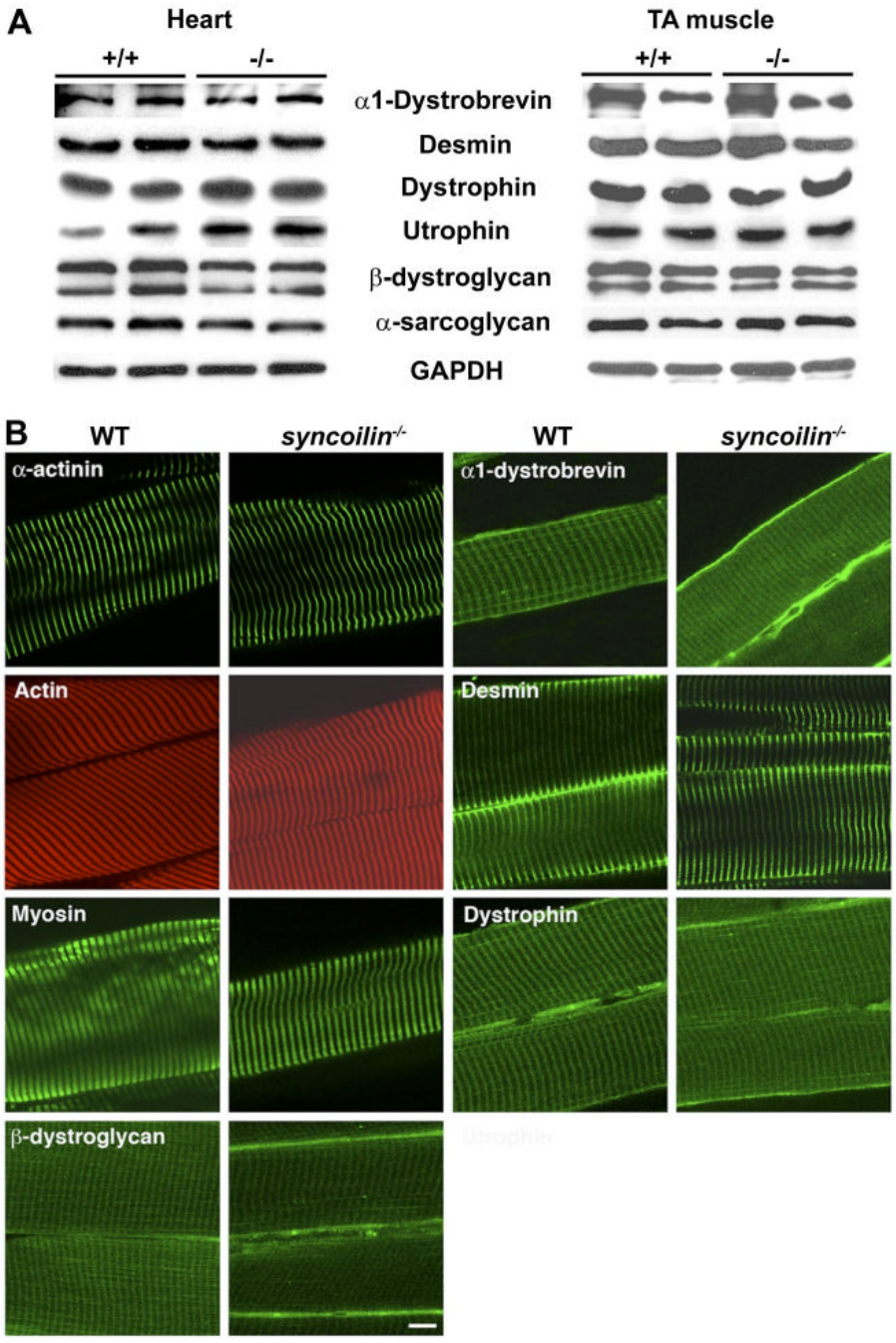

Fig. 3.

Protein expression and localization. *A*: Western blot analyses on heart and TA muscle from 10-wk-old *syncoilin*$^{-/-}$ mice and WT littermates using various antibodies against proteins of the dystrophin-associated protein complex (DPC). *B*: immunostaining of frozen sections of WT and *syncoilin*$^{-/-}$ TA muscle with phalloidin (actin) and antibodies against α-actinin, myosin, β-dystroglycan, α-dystrobrevin, desmin, and dystrophin. Bar, 10 μm.

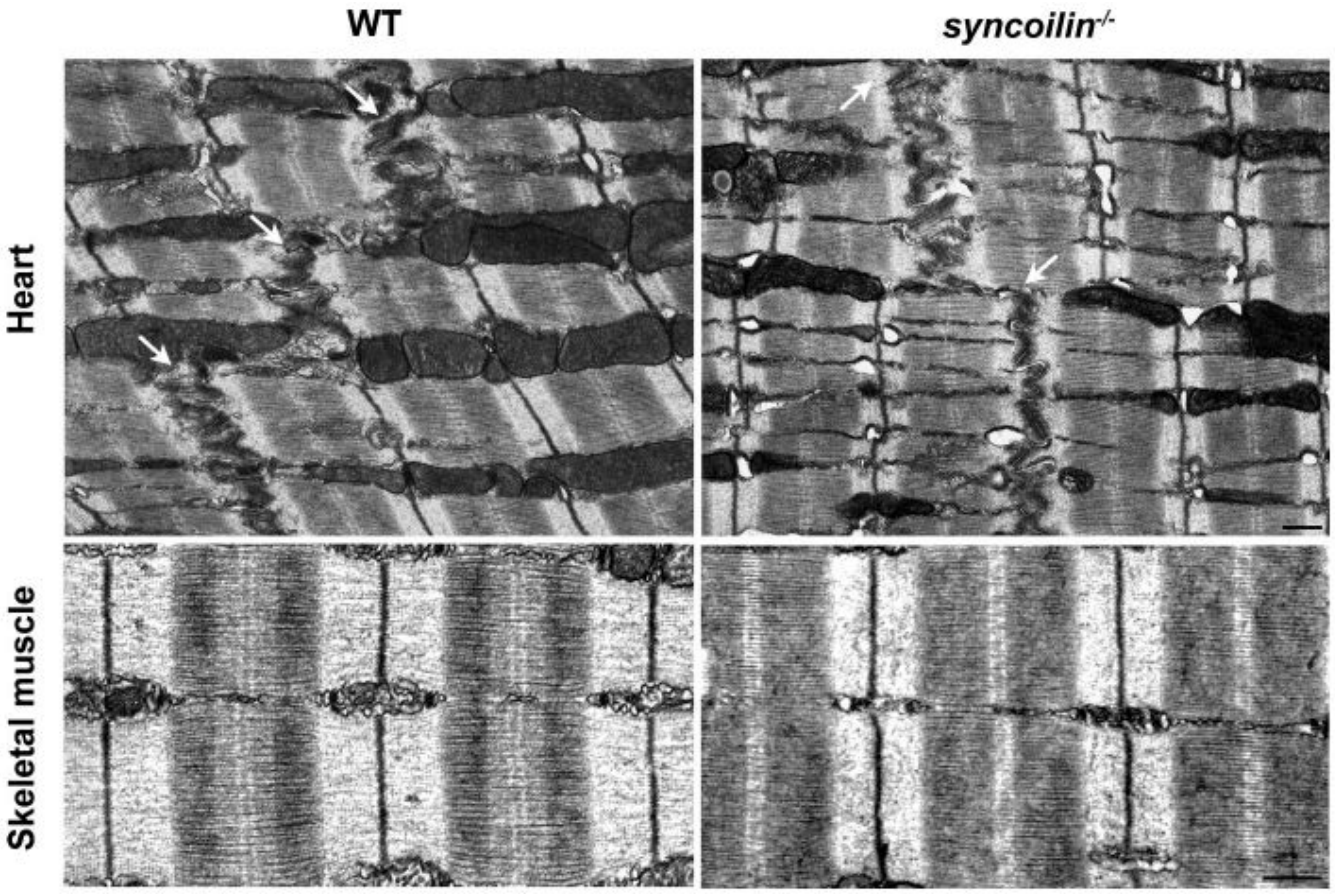

Fig. 4.

Transmission electron microscopy (TEM) of heart and TA muscle from WT and *syncoilin*$^{-/-}$ mice, showing no abnormalities in skeletal and cardiac muscle sarcomeres and cardiac intercalated disks (arrows) in *syncoilin*$^{-/-}$ mice. M, M line; Z, Z line. Bars, 500 nm.

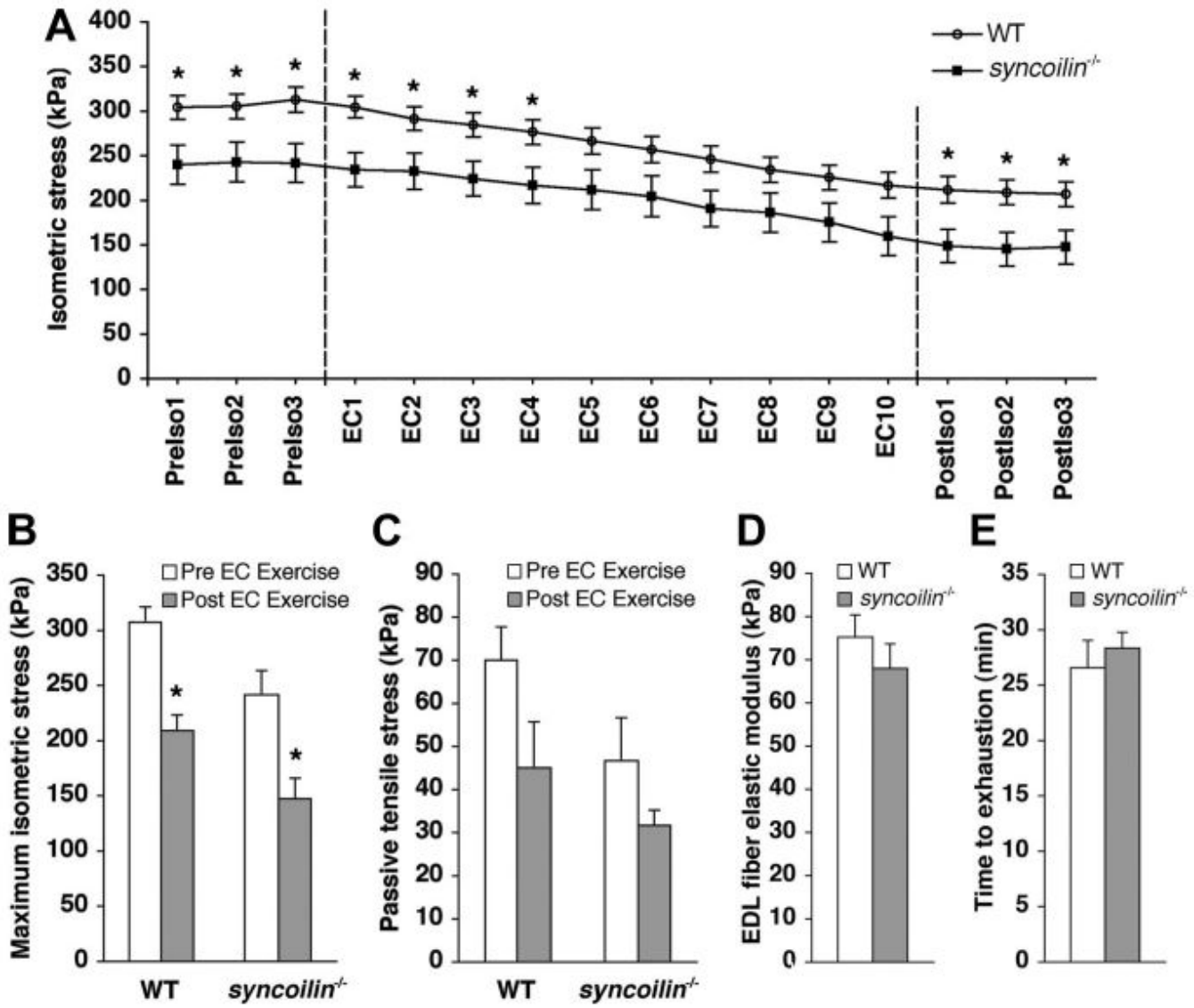

Fig. 5.

Isometric and passive stress generation before and after eccentric contractions (EC). *A*: time course of isometric stress achieved before, during, and after cyclic EC (demarcated by dashed lines). PreIso, isometric stress before the EC protocol; PostIso, isometric stress after the EC protocol. Each symbol represents the mean ± SE of 6 mice per group. *B*: average maximum isometric stress generated by WT and *syncoilin*$^{-/-}$ muscles measured before and after the EC protocol. *C*: passive stress generated by WT and *syncoilin*$^{-/-}$ muscles at a stretch of magnitude equal to 10% of each muscle fiber length. *D*: elastic moduli of WT (n = 21) and *syncoilin*$^{-/-}$ (n = 15) extensor digitorum longus (EDL) muscle fibers. No significant difference in passive stiffness between WT and *syncoilin*$^{-/-}$ fibers was found. *E*: time to exhaustion in treadmill test of *syncoilin*$^{-/-}$ mice (n = 4) and WT mice (n = 4) showed no significant difference in performance. *P < 0.05.

Table 1

Comparative echocardiographic measurements before and 14 days after induction of hypertrophy by TAC

	Before TAC		After TAC	
	WT	***Syncoilin*$^{-/-}$**	**WT**	***Syncoilin*$^{-/-}$**
n	7	7	7	7
Age, wk	8.8±0.2	8.9±0.1	11.0±0.1	11.1±0.1
Body weight, g	28±2	28±2	31±2	31±1
Heart rate, beats/min	478±72	448±101	572±51	518±64
LVIDd, mm	3.92±0.33	3.80±0.20	3.56±0.28	3.88±0.48
LVIDs, mm	2.26±0.40	2.07±0.22	1.98±0.33	2.36±0.68
IVSd, mm	0.56±0.03	0.58±0.04	0.77±0.10	0.72±0.05
IVSs, mm	1.01±0.03	1.02±0.09	1.22±0.09	1.12±0.11
LVPWd, mm	0.58±0.3	0.60±0.03	0.78±0.11	0.73±0.05
LVPWs, mm	1.09±0.11	1.12±0.07	1.32±0.11	1.32±0.15
LV FS, %	42.5±6.8	45.4±5.0	44.7±6.0	40.0±11.5
VCF, circ/s	8.67±1.78	8.94±1.24	8.84±1.10	7.99±2.71
LVMd, mg	73.4±11.7	72.6±7.6	92.8±20.2	98.6±24.4
LVM/BW, mg/g	2.65±0.30	2.62±0.27	3.04±0.61	3.20±0.79
HW/BW, mg/g	N/A	N/A	5.6±0.2	6.0±1.1
PG, mmHg	N/A	N/A	88±6	87±16

Values are means ± SD in wild-type (WT) and syncoilin knockout (*syncoilin*$^{-/-}$) mice. Data comparison was carried out before and after transverse aortic constriction (TAC) in either group. LVID, left ventricular (LV) inner diameter; IVS, interventricular septum; LVPW, LV posterior wall thickness; LV FS, LV fractional shortening; VCF, velocity of circumferential fiber shortening; LVM, LV mass; BW, body weight; HW, heart weight; PG, pressure gradient; d, diastole; s, systole; circ, circumference.

Table 2

Basal cardiac function of syncoilin$^{+/-}$ and WT mice at 10 wk of age as assessed by heart catherization

	WT	*Syncoilin*$^{-/-}$	*t*-Test
Heart rate, beats/min	372±39	349±91	0.582
LVP_{max}, mmHg	132.7±20.5	117.9±30.8	0.349
dP/dt_{max}, mmHg/s	9,207±1,581	8,146±1,026	0.283
dP/dt_{min}, mmHg/s	−7,783±1,613	−7,206±861	0.939
EDP, mmHg	5.1±2.8	6.5±6.8	0.875
Experimental tau, ms	12.0±1.32	11.88±2.62	0.895

Values are mean ± SD in WT (n = 8) and *syncoilin*$^{-/-}$ mice. LVP_{max}, maximum end-systolic LV pressure; dP/dt_{max}, maximum positive first derivative of LVP (contractility); dP/dt_{min}, maximum negative first derivative of LVP (relaxation); EDP, end-diastolic pressure.